Supporting Information

Chanda et al. 10.1073/pnas.1002143107

SI Materials and Methods

Ultrapure 18-MΩ/cm2 water was obtained in-house from a MilliQ water filtration system (Millipore). All chemicals and reagents were used directly without further purification. Transmission electron microscope (TEM) images were obtained on a JEOL 1400 TEM. TEM samples were prepared by placing 5 μL of gold nanoparticle solution on the 300-mesh carbon-coated copper grid and allowed the solution to sit for 5 min; excess solution was removed carefully and the grid was allowed to dry for an additional 5 min. The average size and size distribution of gold nanoparticles synthesized were determined by the processing TEM image using image processing software such as Adobe Photoshop (with Fovea plug-ins). The absorption measurements were done using Varian Cary 50 ultraviolet-visible (UV-Vis) spectrophotometers with 1 mL of gold nanoparticle solution in disposable cuvettes of 10-mm path length. Size and surface charge of gold nanoparticles were measured by differential centrifugal sedimentation (DCS; disk centrifuge, CPS Instruments) and dynamic light scattering (DLS; Malvern Zetasizer) techniques. The University of Missouri Research Reactor irradiation facilities were used for the production of Au-198/Au-199. Animal studies were approved by the Institutional Animal Care and Use Committees of the Harry S. Truman Memorial Veterans Hospital and the University of Missouri, and were performed in accordance with the Guide for the Care and Use of Laboratory Animals.

Synthesis of Starch Stabilized Gold Nanoparticles. The starch stabilized gold nanoparticles (SAuNPs) were prepared by reducing $NaAuCl_4$ with trimeric alanine-based phosphine, $P(CH_2NHCH(CH_3)\text{-}COOH)_3$ (THPAL) in starch at 100 °C. Briefly, 12 mg of starch was dissolved in 6 mL of deionized water (DI) water by heating the mixture at 100 °C for 3 min. A 100-μL $NaAuCl_4$ solution (0.1 M in DI water) was added to the hot starch solution, followed by 20 μL of THPAL solution (0.1 M in DI water) with continuous stirring at 100 °C. The color of the mixture changed from light yellow to dark purple–red within a minute after addition of THPAL, which was an indication of the formation of SAuNPs. The solution was further stirred for 1 min at 100 °C and for 30 min without heating to cool down to room temperature. The cold SAuNP solution was purified by passing through a Sephadex column to remove the unbound starch from the product solution. Finally, the pure SAuNPs were characterized by UV-absorption spectroscopy, DCS, and TEM analysis (Fig. S1).

Purification of SAuNPs. Purification of SAuNPs involved size-exclusion chromatography using a Sephadex G-100 column (Fig. S1). Combinations of UV and TEM were used to characterize the identity of various fractions eluted from the Sephadex G-100 column. After a series of attempts, the chromatography protocol was optimized so that the pure SAuNP fraction eluted as a second purple band from the column (Fig. S1). The identity of this fraction as a well-defined nanoconjugate was further confirmed through UV and TEM data. The hydrodynamic size of SAuNPs as consistently eluted from our purification protocol was 99 ± 2 nm, which is in the range reported for nonaggregated starch encapsulated gold nanparticulate conjugates (1). The nonaggregated and pure SAuNPs as obtained above were used in conjugation reactions with disulfide functionalized BBN peptide (BBN).

Synthesis of ^{198}SAuNPs. Gold leaf (0.76 mg) was irradiated for 3.5 h. The calculated activity of ^{198}Au was 20.5 mCi according to the Capintec CRC-12. The ^{198}Au foil was placed in a liquid scintillation cocktail (LSC) vial and dissolved in 800 μL of aqua regia. The reaction was well shielded by three lead bricks forming a triangle around the reaction vial. The solution was heated to reduce the volume until ≈200 μL was left. A total of 600 μL of 0.05 M HCl was added and heating continued until most of the acid had evaporated. The solution was removed from the hot plate and allowed to cool in a lead pig behind a lead brick followed by the addition of 200 μL of 0.05 M HCl. A 3.75 mg/mL solution of starch was prepared by dissolving 84.4 mg of starch with 22.5 mL of Milli-Q water. The solution was heated and stirred until boiling. A 33.7 mg/mL of THPAL solution was prepared by dissolving 8.7 mg of THPAL in 258 μL Milli-Q water. A total of 18.4 mCi of Au-198 (∼100–200 μL) was transferred to a new LSC vial and 80 μL of cold (0.1 M Au) $HAuCl_4$ carrier was added. Six microliters of hot starch was added, immediately followed by 40 μL of THPAL solution. An immediate color change from yellow to purple–red was observed. The solution was gently swirled and then capped. Sephadex G-100 superfine (300 mg/column) was added directly into the Bio-Rad poly prep column with water and 2 mL of S^{198}AuNP was added to each column. After all of the S^{198}AuNP was adsorbed in the column, 2 mL of Milli-Q water was added and eluted on the basis of the migration of the purple–red band of the nanoparticles. The amount of S^{198}AuNP recovered from each column based on activity is shown in Table S1. The UV-Vis spectrometer was used to characterize prefiltered S^{198}AuNP, filtered S^{198}AuNP from column 1, and filtered S^{198}AuNP from column 2 (Fig. S1).

Synthesis of Thioctic Acid–BBN Peptide. The synthesis BBN was performed using solid phase peptide synthesis employing Fmoc chemistry methodology. A 4-hydroxymethylphenoxyacetyl-4′-methylbenzyhydrylamine resin was used as the solid support for the synthesis. Fmoc-protected amino acids were activated using one equivalent of 0.45 M HBTU/HOBt solutions and two equivalents of N,N-diisopropylethylamine. The amino acids were Fmoc deprotected using piperidine and coupled using NMM.HBTU. Following the coupling of all of the amino acids in the appropriate sequence, thioctic acid (lipoic acid) was coupled using DIC.HOBt. Cleavage of the peptide from the resin was performed using TFA. This cleavage step also removes the amino acid side chain protecting groups. The peptide was purified on a reverse-phase HPLC/C18 column using an AB gradient from 0% B, where A is 0.1% TFA in water and B is 0.1% TFA in acetonitrile. Following purification, the peptide mass was measured by liquid chromatography–mass spectrometry or matrix-assisted laser desorption/ionization, and the purity was measured using HPLC reverse-phase chromatography.

Synthesis of AuNP–BBN Conjugates. The purified SAuNPs were used for conjugation with thioctic-acid–modified BBN with different ratios, e.g., AuNP:bombesin = 1:1, 1:2, and 1:3 for synthesizing AuNP–BBN-1, AuNP–BBN-2, and AuNP–BBN-3, respectively. For AuNP–BBN-1, 5.45 mg of BBN in 1 mL of HPLC-grade methanol was added to 5 mL of SAuNP solution (OD_{535} = 1.75). The mixture was stirred for 12 h at room temperature in a closed round-bottom flask. Reaction kinetics was monitored by disk centrifuge (DCS) technique (Fig. S4). After successful conjugation, the unbound peptide was separated by centrifugation at 10,000 rpm for 10 min in a Fisher AccuSpin 400 microcentrifuge. The pellet obtained was washed three times with HPLC-grade water. In addition, the precipitate was washed with methanol three times and finally dried under vacuum centrifugation. The bombesin-conjugated gold nanoparticles (AuNP–BBN-1) were characterized by UV, TEM, DCS, and DLS techniques (Fig. S2 and

Table 1). The same synthesis procedure was followed for the other conjugates, AuNP–BBN-2 and AuNP–BBN-3, where 10.92 and 16.27 mg of peptide in 1 mL of methanol was used to react with 5 mL of SAuNP solution, respectively.

Synthesis of ^{198}AuNP–BBN Conjugates. The S^{198}AuNPs (OD_{540} = 0.91) from column 1 were used for the BBN conjugation. A total of 1.8 mg of BBN was dissolved with 1 mL of methanol in a 10-mL Hollistier-Stier vial. A total of 1 mL (752 μCi) of filtered S^{198}AuNP was added to the BBN solution and stirred for 12 h. The reaction was well shielded with lead bricks, and the dose rate from the hood was under 1 mR/h. After successful conjugation, the crude ^{198}AuNP–BBN was transferred to a 10-mL centrifuge vial and washed with 2 mL methanol. The activity in the centrifuge vial was 626 μCi. The ^{198}AuNP–BBN was washed three times with methanol by centrifugation technique. The methanol (supernatant) was removed each time and counted for activity (Table S2). After the methanol wash, three washes with Milli-Q water were performed, and supernatant was removed and counted for activity (Table S2). At the end, the final activity was only 109.3 μCi. In an effort to recover more activity, washes 1, 2, and 3 with water were combined and centrifuged again. The supernatant was removed, and the pellet was added to the first collection. Finally, the total activity of ^{198}AuNP–BBN conjugates was 155 μCi. The plasmon resonance of the UV spectrum matches the AuNP–BBN-3 conjugates.

Characterization of AuNP–BBN. We have used the combination of TEM, hydrodynamic size, and x-ray photoelectron spectroscopy to characterize and to confirm the nonaggregated nanoparticulate identity of AuNP–BBN.

In our series of measurements of hydrodynamic sizes, we have confirmed that the increase of the hydrodynamic size of AuNP–BBN conjugates is due to the encapsulation of starch around AuNP–BBN because the precursor AuNP material used in our preparations was stabilized by starch matrix. SAuNPs of very high purity are generated as shown in the detailed synthetic and purification protocols described in the previous sections. Purified SAuNPs showed a hydrodynamic size of ∼99 nm, corroborating values reported in the literature (1). Thioctic acid functionalized-bombesin conjugate (BBN), was treated with purified SAuNPs, resulting in efficient conjugation of SAuNPs with BBN peptide (Scheme 1). This process has been successful with different concentrations of BBN, allowing gold nanoparticles to cover a maximum surface area with bombesin peptide. A series of in vitro studies and x-ray photoelectron spectroscopic (XPS) analysis of AuNP–BBN(1–3) has conclusively indicated effective encapsulation of starch molecules around AuNP–BBN(1–3), rendering excellent biocompatibility and stability against aggregation of nanoparticles. Therefore, the hydrodynamic size measurement of the purified conjugate AuNP–BBN(1–3), which showed an increased size (Table 1), not only corresponds to the conjugation of BBN units on AuNPs (16 ± 5 nm) but also includes the size associated with starch that encapsulates AuNP–BBN (1–3), affording biocompatibility to the nanoconjugates. Our extensive studies have shown that the hydrodynamic size of precursor SAuNPs is 99 ± 2 nm, which corroborates recent literature findings (1). Therefore, hydrodynamic sizes of AuNP–BBN conjugates as observed unequivocally suggested the coexistence of BBN units on AuNPs with effective encapsulation of starch.

To independently confirm the encapsulation by starch molecules onto AuNP–BBN-3, we have subjected the AuNP–BBN–starch conjugate to enzymatic degradation using α-amylase. α-Amylase is expected to digest the carbohydrate linkages in starch molecules, causing substantial reduction in the hydrodynamic sizes of AuNPs. Indeed, treatment of AuNP–BBN–starch conjugate with α-amylase showed enzymatic degradation of starch as the hydrodynamic size of the resulting product showed a reduction of nanoparticulate size to ∼60 nm. These data infer that AuNP–BBN-3 is still bonded to smaller segments of carbohydrates as a result of the digestion of starch by α-amylase. An independent study confirms similar hydrodynamic size changes for SAuNPs when subjected to enzymatic cleavage reactions (1).

Our additional proof for the conjugation of BBN peptide in AuNP–BBN-3 comes from highly reproducible data from IC_{50} measurements of the binding affinity of starch-encapsulated AuNP–BBN-3 with GRP receptors present on prostate cancer cells (Table 1 and Fig. 2). Reproducible IC_{50} values clearly suggest that AuNPs are conjugated to BBN in well-defined stoichiometry/concentration.

Deliberate aggregation of AuNP–BBN-3, which can be effected by refluxing this conjugate in PBS buffer at 100 °C for 1 h, produced aggregated AuNP–BBN-3. Aggregated AuNP–BBN-3 samples did not show any binding affinity toward GRP receptors on prostate cancer cells, thus further inferring that the starch-encapsulated AuNP–BBN-3 nanoconjuagtes used in our in vitro and in vivo investigations are indeed well-defined nonaggregated tumor-specific nanoconjugates. Binding affinity investigations of just the starch-encapsulated gold nanoparticles, SAuNPs, were also performed to test if starch moiety on AuNPs has any effect on the overall binding affinity toward GRP receptors. Results from these experiments revealed the complete absence of binding affinity of SAuNPs toward GRP receptors, thus inferring that starch encapsulation around AuNP–BBN-3 affords only aqueous solubility, biocompatibility, and stability against aggregation and that starch does not contribute toward binding affinity to GRP tumor receptors. Therefore, our results conclusively demonstrate that a biocompatible matrix such as starch has the propensity to encapsulate around AuNPs and offer increased stability to AuNP-3. The hydrodynamic size of 155 nm, as observed in a series of our experiments for AuNP–BBN-3, is due to the incorporation of BBN directly onto the gold nanoparticle surface encapsulated with starch and that starch molecules remain bound to gold nanoparticles. X-ray photoelectron spectroscopic findings as discussed below further confirm the presence of starch around AuNPs and the unaggregated feature of the AuNP–BBN-3 nanoconjugate.

We have performed a systematic investigation to understand the origin of negative zeta potential of AuNP–BBN conjugates. As part of this investigation, our initial focus was to determine the zeta potentials of all of the building blocks of AuNP–BBN conjugate, namely thioctic acid, bombesin, and SAuNP. It is important to note that all of the organic starting materials bear positive zeta potential values and that starch-stabilized AuNPs show negative zeta values. These data indicate that the negative zeta potential in AuNP–BBN conjugate may be due to an intrinsic surface charge on the gold nanoparticle. The "naked" gold nanoparticles bear a negative surface charge (2). On binding with thioctic-bombesin conjugate (SS-BBN) the surface charge will not be completely neutralized. This charge imbalance results in the negative zeta potential of −27.2 mV for AuNP–BBN conjugate. In SAuNPs, the charge on a AuNP is negative; this charge is compensated by the coating of neutral starch molecules, resulting in net negative potential. When the starch layers on AuNPs are replaced by SS-BBN via covalent conjugation, the negative potential of AuNPs is not completely neutralized by the less positive charge bearing SS-BBN conjugate, resulting in the net negative charge for AuNP–BBN conjugate. We therefore believe that the negative zeta potential in AuNP–BBN is predominantly due to surface charge on gold nanoparticles in AuNP–BBN conjugates. A similar observation is noted in the case of the conjugation of gold nanospheres with tumor necrosis factor (TNF). The surface charge on the naked nanosphere is estimated to be approximately −38 mV and, upon conjugation with TNF, the zeta potential shifts to −34.55 mV (2).

To unambiguously establish the structural details relating to unaggregated features of AuNP–BBN-3, we performed detailed XPS measurements.

Relative Elemental Composition. Using XPS measurements, we have determined the relative elemental composition of C, N, O, and S in AuNP–BBN-3. The experimental atomic ratio of N/S = 13/2.6 is consistent with the calculated ratio of N/S = 13/3 (other values are shown in Table S3). On the basis of these data it is clear that the bombesin peptide is present and conjugated to gold nanoparticles. However, on the basis of the observed data for O/S and C/S ratios, it is clear that starch molecules are present in the nanoconjugate AuNP–BBN-3. The starch molecules encapsulate the AuNP–BBN construct and provide additional stability.

The XPS high-resolution spectrum of the C1s region shows various N-C = O, C = O, C-O, C-N, and C-C and C-H regions as expected from conjugated bombesin peptide (Fig. S4). The S2p region exhibits two distinct sulfur peaks at 164.1 and 165.3 with a ratio of 2:1 corresponding to Au-S (sulfur coordinated to AuNPs) and methylcystine (S-CH3) corresponding to sulfur present in the methylcysteine amino acid in the BBN peptide backbone (Fig. S4). Each class of sulfur peak was further split into the doublet S2p3/2 and S2p1/2 with coupling of 1.2 eV, which is in agreement with the literature values (3, 4). Because no further peaks are observed in the higher energy region of the spectrum corresponding to oxidized sulfur, these measurements are consistent with the observation that the AuNP–BBN is the exclusive product formed during the nanoconjugation reaction. In the Au 4f region of the spectrum, two different gold with energies (84.7 and 88.4; 89.5, and 85.8) corresponding to Au(0) and surface gold with partial Au(I) character were observed (Fig. S6). It is widely believed from various recent studies that disulfide in thioctic acid oxidatively adds to AuNPs, resulting in a partial Au(I) character at the surface of the nanoparticle (4). Energy of ~85 eV for the Au 4f7/2 peak suggests that the Au is bound to S. Consistent with this fact, two different oxidation states of gold corresponding to surface and core gold atoms are noted in the XPS spectrum. Results from various XPS studies on gold nanoparticles confirm similar findings (5). The above observations unequivocally establish the unaggregated identity of AuNP–BBN-3 nanoconjugate.

In Vitro Stability Studies of AuNP–BBN Conjugates. In vitro stability studies were performed on bombesin-conjugated gold nanoparticles, AuNP–BBN-1, AuNP–BBN-2, and AuNP–BBN-3 by mixing to the aqueous solutions of 10% NaCl, 0.5% cysteine, 0.2 M histidine, 0.5% human serum albumin (HSA), 0.5% BSA, or 0.2 M DTT (Fig. S3). The stability of the conjugates was measured by monitoring the UV absorbance over 24 h. A negligible change in plasmon band was observed in UV for Au–BBN-3, which confirmed the retention of nanoparticulate composition in all of the mixtures. In vitro stability studies after 24 h of treatment of AuNP–BBN-1, AuNP–BBN-2, and AuNP–BBN-3 with NaCl are shown in Fig. S3.

Cell Culture and Receptor Binding (IC_{50}) Assays. PC-3 prostate cancer cells were obtained from the American Type Culture Collection (ATCC). PC-3 cells were maintained in RPMI medium supplemented with 4.5 g/L D-glucose, 25 mM Hepes, 0.11 g/L sodium pyruvate, 1.5 g/L sodium bicarbonate, 2 mM L-glutamine, 10% FBS, and antibiotics. The receptor binding affinity (IC_{50}) of bombesin-conjugated gold nanoparticles (Au–BBN) was determined by a competitive cell-binding assay on PC-3 cells in cultures using ^{125}I-Tyr4-bombesin as the GRP-specific radioligand. Approximately 30,000 cells were incubated at 37 °C for 40 min under 5% CO_2 in the presence of 20,000 cpm ^{125}I-Tyr4-bombesin (2,200 Ci/mmol) and increasing concentration of AuNP–BBN conjugates (Fig. S3). After incubation, the reaction medium was aspirated, and the cells were washed three times with cold RPMI 1640 modified buffer. Cell-associated radioactivity was determined by counting in a Packard Riastar γ counting system. IC_{50} values were calculated using GraphFit 4.0 graphing software. The percentage of ^{125}I-Tyr4-bombesin bound to cells was plotted against increasing the concentration of AuNP–BBN conjugates to determine the IC_{50} values.

Cellular Uptake of Bombesin-Conjugated Gold Nanoparticles. PC-3 cells were used for the in vitro cell internalization analyses. TEM was used to visualize the gold nanoparticles inside the cells. Known concentrations of gold bombesin nanoconjugates (3 mg/mL) were added to 5 mL DMEM (10% FBS, 1% penicillin/streptomycin), and cells were incubated for 4 h at 37 °C. Following incubation, cells were washed thoroughly with medium followed by PBS for five times and were dislodged using trypsin –EDTA solution followed by a single wash with complete medium and two washes with PBS (pH 7.4) to remove unbound AuNP–BBN conjugates. The cell pallets were fixed with 2% glutaraldehyde/2% paraformaldehyde in sodium cacodylate buffer (0.1 M). The cells were post-fixed with 1% buffered osmium tetraoxide and dehydrated in a graded ethanol series before embedding in Epon–Spurr epoxy resin. Sections (75–85 nm) were cut using Leica Ultracut UCT ultramicrotome and placed on a TEM grid. The sections were poststained with uranyl acetate and lead citrate for organelle visualization. The prepared samples were viewed with the JEOL 1400 TEM.

Biodistribution of AuNP–BBN-3 in Normal Mice Model. The biodistribution of bombesin-conjugated gold nanoparticles AuNP–BBN-3 was assessed in a group of two normal mice weighing ~20 g. The amount of gold present in various organs was estimated using the neutron activation analysis (NAA) technique. The animals were injected through i.p. (187 μL, 1 mg/mL of AuNP–BBN-3) and killed after 24 h. The amount of gold in pancreas, kidney, spleen, lung, and liver was determined to assess the receptor binding affinity for AuNP–BBN-3 in vivo.

Sample Preparation for NAA. Samples were prepared by placing the tissue into precleaned, high-density polyethylene irradiation vials. The weight of each sample was recorded, and the vial was capped. Blanks, duplicates, and spiked samples were included in the NAA sample sets.

NAA Analysis. Samples were loaded in polyethylene transfer "rabbits" in sets of nine and were irradiated for 90 s in a thermal flux density of $\approx 5 \times 10^{13}$·ncm^{-2}·s^{-1}. The samples were then allowed to decay for 24–48 h and counted in real time for 1200 s at a sample-to-detector distance of ≈5 mm. The spectrometer consisted of a 21% high-purity germanium detector with a full-width-at-half-maximum resolution of 1.8 keV at 1331 keV and a Canberra 9660 digital signal processor. Dead times ranged from 1 to 11%. The mass of gold was quantified by measuring the 411.8 keV gamma ray from the β^- decay of ^{198}Au ($t_{1/2}$ = 2.7 days). The area of this peak was determined automatically with the Genie ESP spectroscopy package from Canberra. Nine geometrically equivalent comparator standards were prepared by pipetting ≈0.1 mg of gold from a 10.0 ± 0.5-μg/mL certified standard solution (High-Purity Standards) on paper pulp in the polyethylene irradiation vials. Analysis of the gold comparator standards yielded a relative specific activity (average and standard deviation) of 237,239 ± 6,084 counts/μg Gd (n = 9) with a relative standard deviation of 2.6%.

Biodistribution of ^{198}AuNP–BBN in Severe Combined Immunodeficient Mice. Animal studies were approved by the Institutional Animal Care and Use Committees of the Harry S. Truman Memorial Veterans Hospital and the University of Missouri and were performed in accordance with the Guide for the Care and Use of Laboratory Animals. Female ICRSC-M severe combined immunodeficient (SCID) mice (4–5 weeks of age; Taconic Farms) were group housed in a temperature and humidity controlled pathogen-free barrier facility. Animals were maintained on a 12-h light–dark cycle and had access to sterilized standard chow and water ad libitum. Animals were allowed to acclimate for 7–10 days before initiation of work.

The human prostate cancer cell line PC-3 was obtained from the ATCC and cultured according to ATCC recommendations by the University of Missouri Cell and Immunobiology Core Facility. Mice underwent inhalational anesthesia (isoflurane/oxygen) followed by received bilateral s.c. hind-flank inoculations of 10×10^6 PC-3 cells suspended in 0.1 mL of sterile Dulbecco's PBS (DPBS) and Matrigel (2:1, vol:vol). Solid tumors were allowed to develop over a period of 3–4 weeks. Five groups of animals ($n = 5$) each received i.p. injections of ^{198}AuNP–BBN-3 (3.5 μCi) in 100 μL DPBS while under inhalational anesthesia. Radiotracer uptake and retention were determined after 30 min and 1, 2, 4, and 24 h. Mice were euthanized by cervical dislocation, and blood samples were collected by cardiac puncture. Samples of tumor, liver, spleen, pancreas, and other organs of interest from the treatment group were harvested, weighed, and counted for radioactivity using an automated γ-counter to determine the percentage of injected dose per gram and per organ at each time point. Data were evaluated for uptake and clearance and for the uptake specificity.

CT Imaging Using Mice Model. Female NCR nudes were obtained from Taconic Farms. They were 5–6 weeks old on day 1 of the experiment. The animals were fed irradiated Rodent Diet 5053 (LabDiet) and water ad libitum. Mice were housed in Thoren microisolator caging with Bed-O'Cobs bedding. All treatments, body weight determinations, and tumor measurements were carried out in laminar down-flow cabinets. The environment was controlled to a temperature range of 70 ± 2 °F and a humidity range of 30–70%.

PC-3 cells were obtained from the ATCC and cultured in Ham's F-12 media (Mediatech) supplemented with 10% FBS (Invitrogen) and 1% penicillin/streptomycin/glutamine (Mediatech) in T175 cell-culture-treated flasks (Nunc) in humidified 5% CO_2 37 °C incubators. Cells were grown to 80–90% confluency before detachment with trypsin/EDTA (Mediatech) and passaged into new T175 flasks at a split ratio of 1:3 every 3–4 days. On the day of implant, cells were harvested with trypsin/EDTA, which was subsequently neutralized with complete media and collected by centrifugation at 200 × *g*. The cells were washed once with serum-free media and resuspended at a final concentration of 2.5×10^7 cells/mL in 50% serum-free media/50% Matrigel.

Test animals were implanted s.c. high in the axilla on day 0 with 5×10^6 cells with Matrigel (1:1) using a 27-gauge needle. All animals were observed for clinical signs at least once daily. Animals with tumors in excess of 1 g or with ulcerated tumors were euthanized, as were those found in obvious distress or in a moribund condition.

Treatment. Treatments began on day 9, when the mean estimated tumor mass for each group was 126 mg. All animals weighed ≥21.3 g at the initiation of experiments. Mean group body weights at first treatment were well matched (range: 24–24.7 g). All animals were dosed with 100 μL of Au–BBN-3 dissolved in 1× PBS (3 mg/mL). The animals were dosed a total of six times over the course of 2 days to give the tumors maximal exposure to the compound. The doses were given immediately after the prescan and then 2, 5, 8, 23, and 47 h afterward.

Micro-CT imaging. Micro-CT was performed in all mice immediately before treatment and then 1, 6, 24, and 48 h after the start of treatment. A GE RS150 small animal micro-CT scanner was used with the following settings: (*i*) x-ray tube voltage = 70 kVp, (*ii*) x-ray tube current = 25 mA, (*iii*) exposure time = 20 ms, (*iv*) number of frames = 500, (*v*) angle increment between frames = 0.4°, (*vi*) number of averages per frame = 2, and (*vii*) the acquisition method of Parker. Images were initially reconstructed at low resolution, allowing smaller crop volumes to be defined. Images were then reconstructed at higher resolution (250 μm; isotropic) to allow optimal determination of potentially subtle contrast enhancement. The mean tumor CT number was calculated within a volume of interest that was manually defined in Amira.

Assessment of side effects. All animals were observed for clinical signs at least once daily. Individual body weights were recorded on the first day of treatment. Treatment-related weight loss in excess of 20% is generally considered unacceptably toxic. In this report, a dosage level is described as tolerated if treatment-related weight loss (during and 2 weeks after treatment) is <20% and mortality during this period in the absence of potentially lethal tumor burdens is ≤10%. Upon death or euthanasia, all animals were necropsied to provide a general assessment of the potential cause of death and perhaps target organs for toxicity. The presence or absence of metastases was also noted. Clinical signs and necropsy findings were observed.

Tumor growth/general observations/controls. The mean estimated tumor burden for each group in the experiment on the first day of treatment (day 9) was 126 mg. All animals weighed ≥21.3 g at the initiation of therapy. Mean group body weights at first treatment were also well matched (range: 24.0–24.7 g). Thioglycolate cultures of the cells used for implantation of this study were negative for gross bacterial contamination. On the basis of historical data for this model, the biology of the control group was judged to be within the normal range.

Toxicity. There were no treatment-related deaths during the study. There were no clinical signs and no remarkable necropsy findings in this experiment.

1. Deka J, Paul A, Ramesh A, Chattopadhyay A (2008) Probing Au nanoparticle uptake by enzyme following the digestion of a starch-Au-nanoparticle composite. *Langmuir* 24:9945–9951.
2. Paciotti GF, et al. (2004) Colloidal gold: A novel nanoparticle vector for tumor directed drug delivery. *Drug Deliv* 11:169–183.
3. Mukherjee P, et al. (2007) Potential therapeutic application of gold nanoparticles in B-chronic lymphocytic leukemia (BCLL): Enhancing apoptosis. *J Nanobiotechnology* 5:4.
4. Roux S, et al. (2005) Synthesis, characterization of dihydrolipoic acid capped gold nanoparticles, and functionalization by the electroluminescent luminol. *Langmuir* 21: 2526–2536.
5. Brust MWM, Bethell D, Schiffrin DJ, Whyman R (1994) Synthesis of thiol-derivatised gold nanoparticles in a two-phase liquid–liquid system. *J Chem Soc Chem Commun* 1994:801–802.

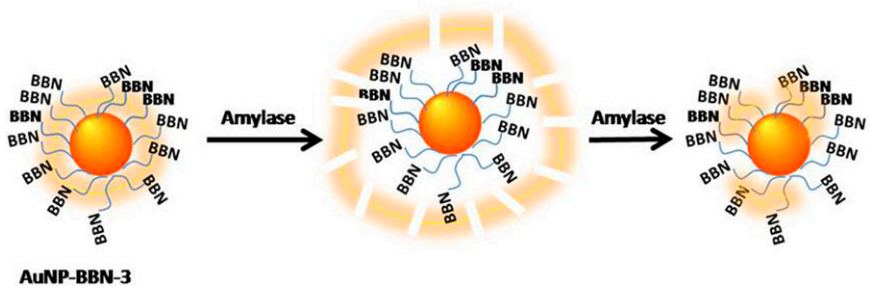

Scheme S1. Schematic representation of enzymatic degradation of AuNP–BBN–starch conjugate.

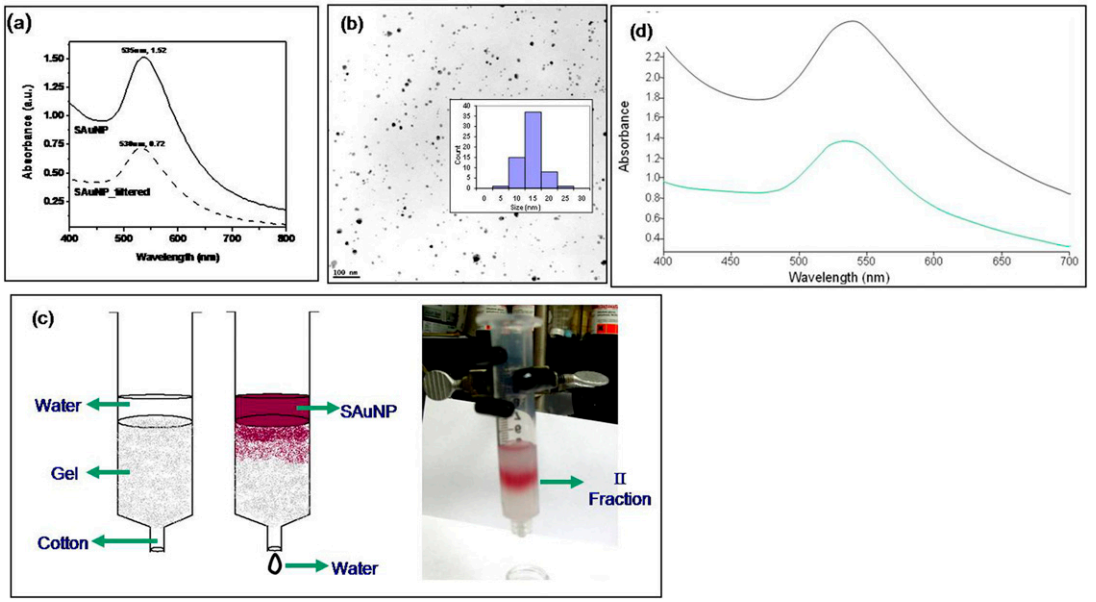

Fig. S1. Characterization of SAuNPs. (*A*) Plasmon absorption spectrum. (*B*) TEM image (*Inset*: particle size distribution). (*C*) Filtration of AuNPs through Sephadex G-100 column to collect different fractions of gold nanoparticles; second fraction alone is used for bioconjugation with SS–BBN. (*D*) UV-Vis spectrum of prefiltered S^{198}AuNP (black) and filtered S^{198}AuNP (green).

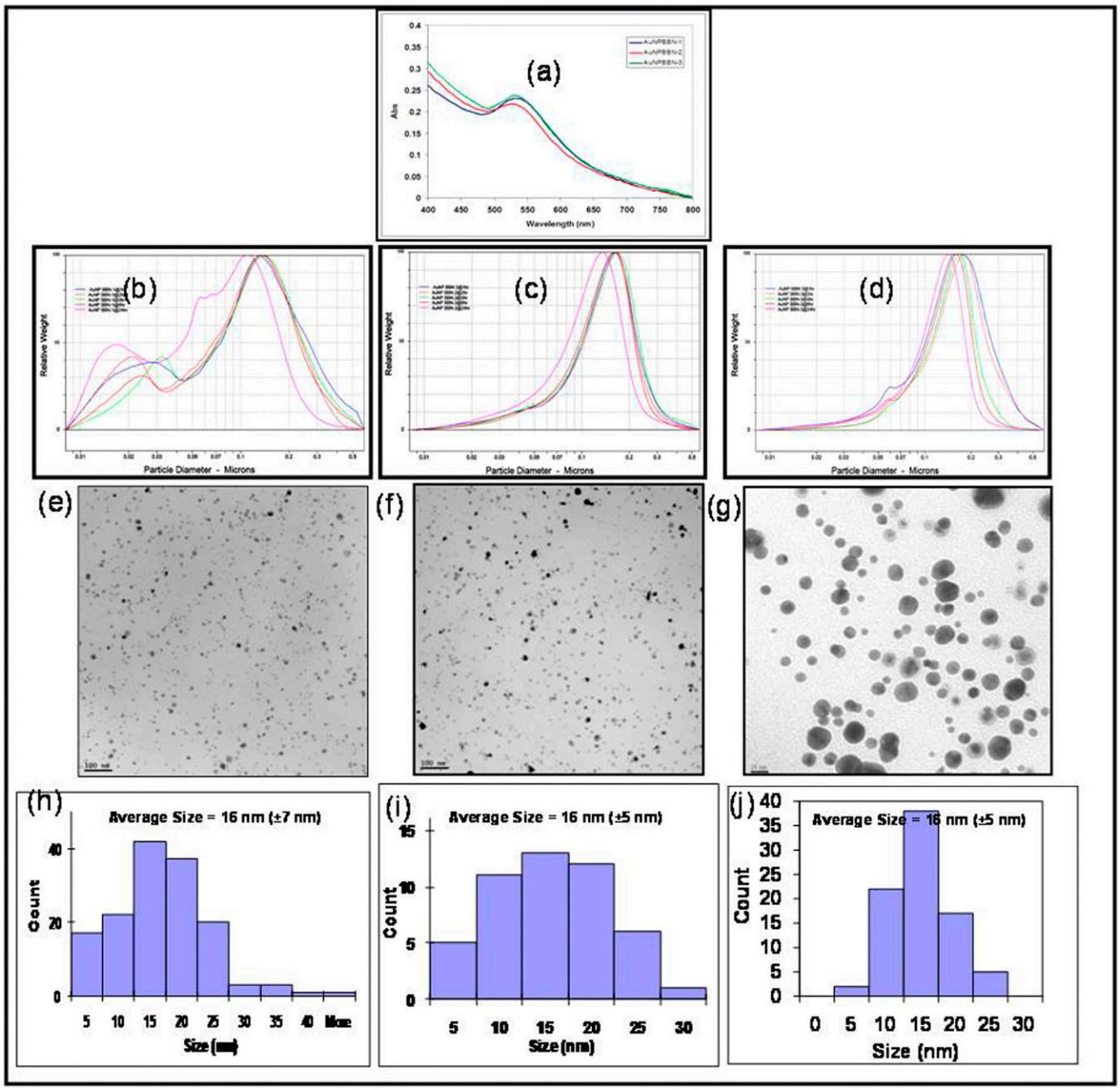

Fig. S2. Library of GRP-receptor–targeting gold nanoparticles: AuNP–BBN-1, AuNP–BBN-2, and AuNP–BBN-3. (*A*) Overlapping absorption spectra of all of the constructs. (*B–D*) Optimization ratio of BBN and SAuNPs by monitoring the size of functionalized gold nanoconstructs AuNP:BBN (1:1), AuNP:BBN (1:2), and AuNP:BBN (1:3) at 1-, 2-, 3-, 6-, and 12-h time intervals. (*E–G*) TEM images of Au–BBN conjugates. (*H–J*) Size histogram of Au–BBN conjugates indicating a 16 ± 5-nm core size.

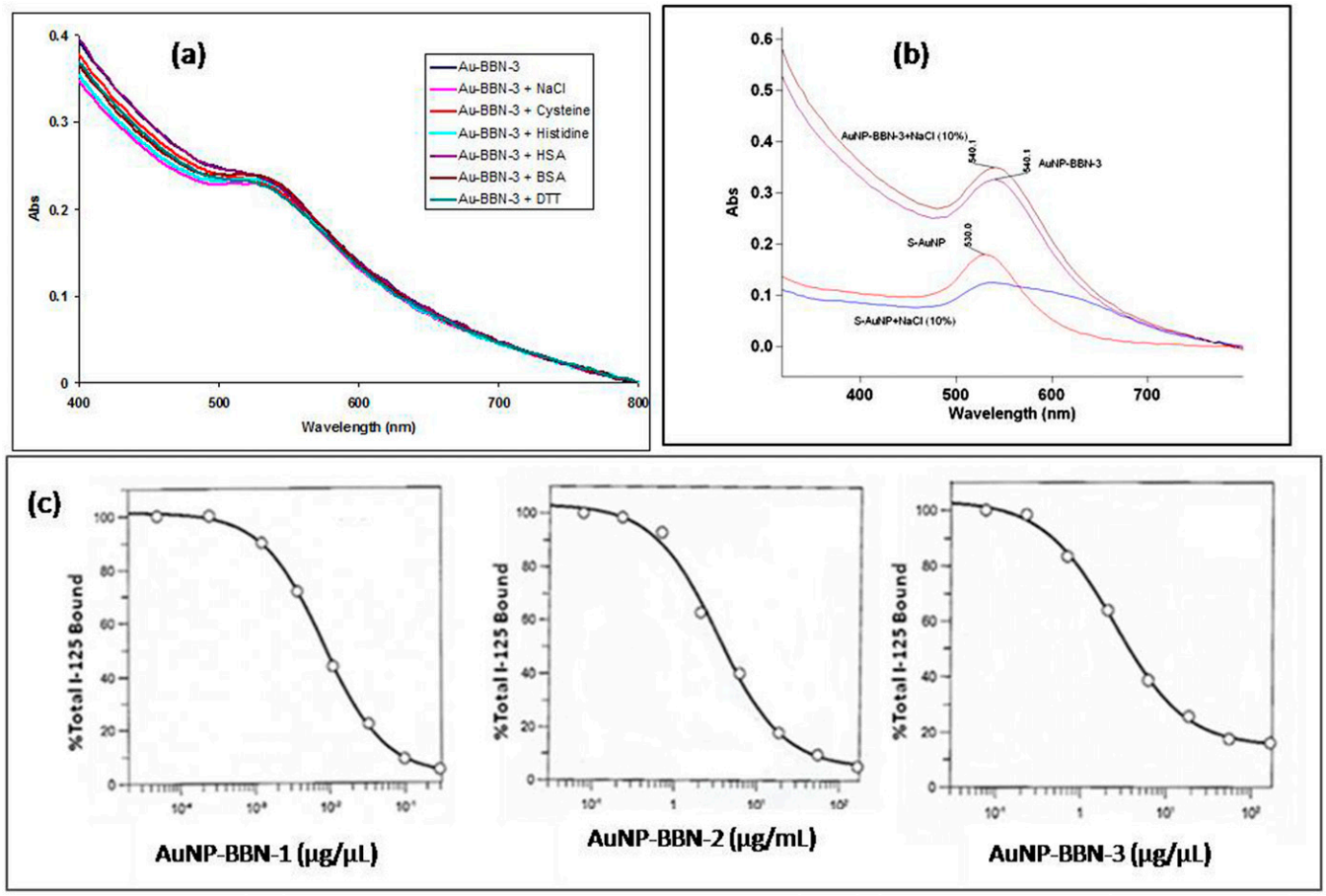

Fig. S3. (*A*) In vitro stability studies of AuNP–BBN-3 conjugates were investigated in biologically relevant solutions. For example, aqueous solutions of AuNP–BBN-3 conjugate were treated with 10% NaCl, 0.5% cysteine, 0.2 M histidine, 0.5% HSA, 0.5% BSA, or 0.2M DTT solutions. (*B*) In vitro stability studies after 24 h treatment of AuNP–BBN-3 and SAuNP with 10% NaCl. (*C*) IC_{50} determination of AuNP–BBN-1, AuNP–BBN-2, and AuNP–BBN-3.

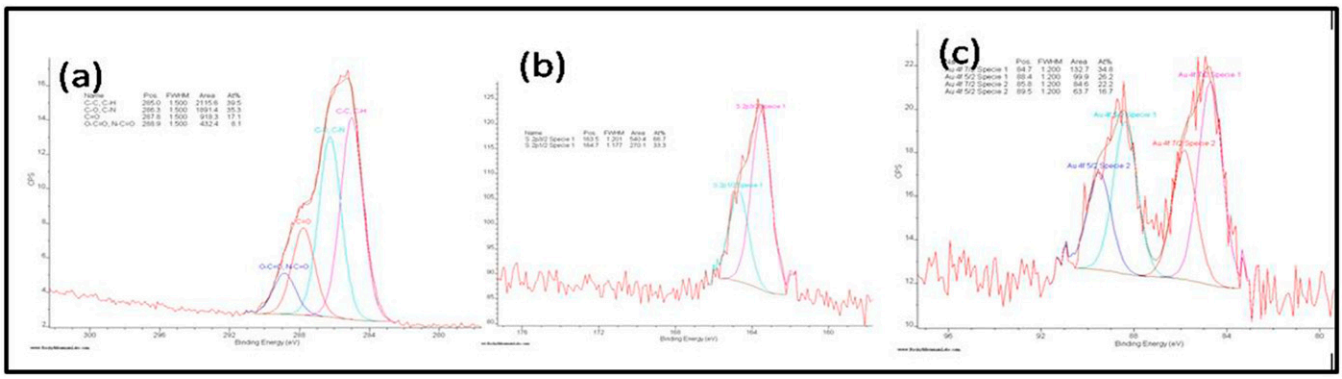

Fig. S4. High-resolution XPS spectrum of AuNP–BBN-3 (*A*) C1s region, (*B*) S2p region, and (*C*) Au4f region.

Table S1. Amount of S^{198}AuNP recovered from columns

S^{198}AuNP	Eluted activity (mCi)	Column bound activity (mCi)	Percent recovered	λ_{max}	Absorption
Prefiltered S^{198}AuNP	—	—	—	550	0.9744
S^{198}AuNP from column 1	1.50	3.90	27.8	540	0.9131
S^{198}AuNP from column 2	1.52	3.83	28.4	540	0.9155

Amounts were determined on the basis of activity counted and the wavelengths and absorbance of prefiltered S^{198}AuNP, filtered S^{198}AuNP from column 1, and filtered S^{198}AuNP from column 2 from UV-Vis spectroscopy.

Table S2. The activity recovered from methanol and water supernatant during washing of ^{198}AuNP–BBN

	Activity in methanol/water washes		
Solvents	Wash 1	Wash 2	Wash 3
Methanol	0.5 μCi	5.0 μCi	5.5 μCi
Water	356 μCi	69.7 μCi	56 μCi

Table S3. Relative elemental composition of AuNP–BBN-3

Ratio	Experimental	Calculated
N/S	13/3	13/3
C/S	64/3	51/3
O/S	18/3	10/3